Journal of Statistical Mechanics: Theory and Experiment

PAPER • OPEN ACCESS

Pedestrian flow analysis in high-density crowds: continuity equation with Voronoi-based fields

To cite this article: Juliane Adrian *et al J. Stat. Mech.* (2026) 043401

OPEN ACCESS

Journal of Statistical Mechanics: Theory and Experiment
An IOP and SISSA journal

PAPER: Interdisciplinary statistical mechanics

Pedestrian flow analysis in high-density crowds: continuity equation with Voronoi-based fields

Juliane Adrian[1,*], **Ann Katrin Boomers**[1], **Sarah Paetzke**[1] **and Armin Seyfried**[1,2]

[1] Institute for Advanced Simulation 7: Civil Safety Research, Forschungszentrum Jülich, Jülich, Germany
[2] Faculty of Architecture and Civil Engineering, University of Wuppertal, Wuppertal, Germany
E-mail: j.adrian@fz-juelich.de

Received 24 June 2025
Accepted for publication 11 February 2026
Published 15 April 2026

CrossMark

Online at stacks.iop.org/JSTAT/2026/043401
https://doi.org/10.1088/1742-5468/ae458a

Abstract. Since the beginning of the century, it has been possible to precisely capture trajectories of pedestrian streams from video recordings. To enable measurements at high density, the heads of pedestrians are marked and tracked, thereby providing a complete representation of the phase space. However, the classical definitions of flow, density, and velocity of pedestrian streams are based on different segments in phase space. In addition, traditional methods fail with high densities of people, as heads move even when a crowd is blocked and standing still. In this study, Voronoi decomposition was used to construct density and velocity fields from pedestrian trajectories to solve this problem. Combined with the continuity equation, a flow equation based on trajectories was derived, exactly satisfying the conservation of particle numbers. The proposed method allows all quantities to be defined within the same segment of phase space, even at scales smaller than the dimensions of a pedestrian. It is shown that these new

[*] Author to whom any correspondence should be addressed.

definitions of flow, density, and velocity are consistent with classical measurements and enable the determination of standstill in pedestrian flows, even when individual body parts are moving. These properties allow inconsistencies in the state of the art of pedestrian fundamental diagrams to be scrutinised.

Keywords: traffic and crowd dynamics, traffic models

Contents

1. Introduction

Density, flow, velocity, and speed are helpful in quantitatively describing collective phenomena and the transport properties of a crowd. They are used as variables for modelling crowd dynamics and for characterising states with respect to risks and comfort. In addition, these quantities are empirically interrelated. The relationship between these quantities gained by empirical measurements is referred to as a fundamental diagram. Different representations, such as speed–density, flow–density, and flow–speed, are used. These relationships facilitate the categorisation of system states, such as congested or free-flow regime. In addition, the fundamental diagram specifies states that are also relevant to crowd safety. In particular, it enables the determination of the density or density regime in which congestion builds up, movement comes to a standstill, and crowding, clogging, or pushing may occur.

Irrespective of empirical relationships, various theoretical concepts and models link speed v, density ρ, and flow J through functions or conservation laws. In pedestrian dynamics, the classical flow equation $J = \rho\, v\, w$, where w denotes the width of the facility, is presented in every textbook [1–4] and applied in practice [5, 6]. In general, these quantities are related to discrete representations of the system, usually the trajectories describing the movement of the pedestrians. Although the flow equation is widely used in practice, it raises fundamental questions. For example, it links quantities such as flow, an average value over time at a fixed cross section in space, with density, usually an average value over space at a fixed point in time. These quantities, therefore, relate to different areas in phase space.

An important reference point in traffic flow theory to address this problem is the method of Edie [7]. The definitions of Edie inherently rely on a combination of spatial and temporal averaging, which does not permit truly localised measurements. In fact, this mixing of averages may obscure stop-and-go states by blending them into the values of density, flow, or velocity. This mixing is particularly relevant because the system is roughly granular, but local measurements are required to identify stop states.

In mathematics or physics, many macroscopic models are based on the continuity equation and on model functions for the fundamental diagram (see [8, 9] or the review [10]). Here, density $\boldsymbol{\rho}(\vec{x},t)$ and velocity $\vec{\mathbf{v}}(\vec{x},t)$ are space-dependent and time-dependent continuous fields. The continuity equation is a conservation law describing changes of density and velocity in time and space, ensuring that no pedestrian in the system is born or turns to dust.

To summarise, the following could be stated. There are different relationships between the central variables to describe transport and safety risks in crowds: (a) empirical measurements of speed, density, and flow as well as the fundamental diagram; (b) the flow equation; and (c) the continuity equation describing transport in moving crowds while conserving the number of pedestrians. However, there is currently no standard in the scientific community for the definition of measured and model variables.

In the following, we introduce the state of the art in data capturing and empirical measurements of density, velocity, and flow; examine the completeness and inconsistencies in determining the fundamental diagram; and discuss how these inconsistencies are related to the continuity or flow equation.

Before the turn of the millennium, quantitative data collection predominantly depended on manual methods (e.g. [11, 12]) or labour-intensive analysis of photographic and video materials (e.g. [13, 14]). The emergence of high-resolution video recording technology for the consumer market significantly facilitated the detailed and efficient documentation of experiments and field studies through video recordings.

To solve the problem of occlusion in experiments with high density, overhead recordings are made. The position of the head is projected onto the ground, providing two-dimensional trajectories. These precise head trajectories formed the basis for microscopic analysis; the development of new measurement methods and representations of density, speed, and flow; and the examination of how the measurement method influences the quantities and their statistical properties [15–19].

Previous approaches to quantifying pedestrian flow and density are often based on definitions that implicitly violate the continuity equation. In particular, inaccuracies arise from inconsistent averaging or from neglecting negative velocity components. This article shows that the new precision in trajectories highlights weaknesses and ambiguities in the classic definitions of key variables used to describe transport properties in crowds. The core objective of our study is to establish mathematical exactness and uniqueness of the mapping from trajectories to fields to gain rigorous definitions of density, flow, and velocity that are consistent with the continuity equation while enabling localised measurements in space and time. These definitions allow the construction of fundamental diagrams that accurately distinguish stop-and-go states and remain consistent with the continuity equation.

This provides a unified and locally valid framework consistent across scales.

The state of the art regarding the fundamental diagram, along with a discussion of inconsistencies and open questions, is presented in section 2.1. Section 2.2 introduces both microscopic and macroscopic representations of the variables based on head trajectories. In section 3.1, the continuity equation is used to relate direct measurements of the flow to a flow calculated using the flow equation, which is in accordance with the continuity equation. The Voronoi decomposition is used to connect the continuity equation, a field equation, with the discrete representation of moving pedestrians by trajectories. In sections 3.2 and 3.3, the framework is used to introduce a flow equation in accordance with the continuity equation and tested by analysing experiments on unidirectional and bidirectional streams. In section 4, the impact of varying definitions of quantities and the absence of precision in notation on the values obtained is analysed.

2. State of the art for measuring transport properties

As outlined at the beginning, the fundamental diagram is of central importance to describe transport in crowds. This section highlights open questions and contradictions in the state of the art. The second part of the section discusses how these problems relate to the definition of variables.

2.1. Fundamental diagram

Numerous empirical studies have shown that fundamental diagrams depend on human factors, such as body height, gender, and culture. The influence of anisotropy of the moving direction (bidirectional or multidirectional streams) and the type of spatial boundaries (such as corridors, intersections, and stairs) has been studied. For an overview on this subject, see [20] or the collection of empirical studies [21, 22]. Numerous studies, including ours, have analysed these influences by comparing fundamental diagrams that are not based on the same measurement method. Problems in this context were discussed in [23] for single-file movement. This study used microscopic trajectories from one experiment to measure mean values of density, speed, and flow. The flow equation was used to compare different representations of the fundamental diagram. However, the comparison obtained by the flow equation resulted in inconsistent shapes of the fundamental diagram. The flow equation relates mean values over space at a fixed time, such as density, with mean values over time at a fixed position, such as flow. This leads to discrepancies in the relationship between empirical measurements at high densities, in which the heterogeneity of the system, e.g. due to stop-and-go waves, is pronounced. In the following, we focus on the data incompleteness and inconsistencies resulting from the definitions of speed, density, and flow. Further studies on the measurement methods of speed, density, and flow based on trajectories revealed a significant

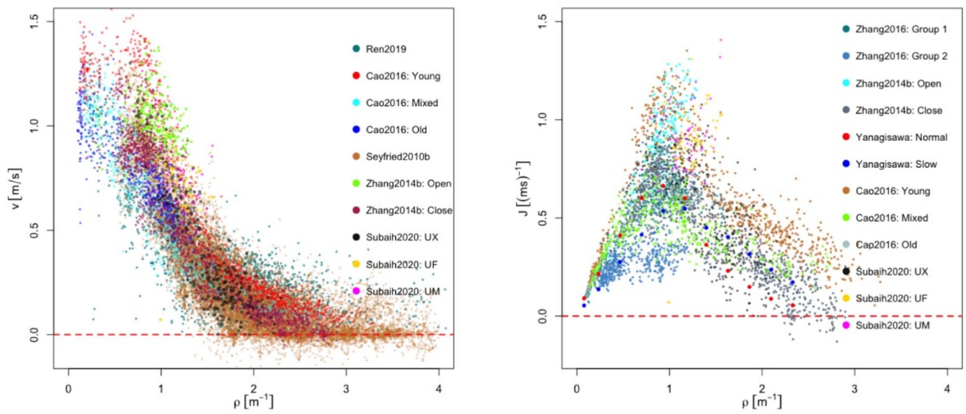

(a) (b)

Figure 1. Fundamental diagrams for single-file experiments: (a) velocity–density and (b) flow–density.

influence on both the shape and fluctuation of the data, even in systems with larger degrees of freedom to move [17–19].

Without any claim to completeness, we next focus on data from experiments conducted under laboratory conditions on single-file, unidirectional, and bidirectional flow in straight corridors. The collection includes studies that cover the density range as complete as possible. All experiments differ in the spatial boundaries of the setup, the test persons, and the initial conditions at the start. Only experiments without additional obstacles in the corridor and without using further accessories, such as mobile phones or luggage, are considered.

Figure 1 shows data from various single-file experiments [24–34]. The compilation shows that the flow of people can come to a complete standstill at high densities, and the velocity as a scalar can even reach negative values.

In other words, these negative scalar velocity values indicate a movement opposite to the main direction of movement.

Three types of stream directions in a corridor are considered in the following: unidirectional streams [17, 18, 35–37], bidirectional streams with two clearly separated stationary lanes [18, 35, 38], and bidirectional streams with multiple intersecting bands changing in space and time [35, 37, 38]. The respective data are shown in figure 2. Data collection includes experiments covering the density range as completely as possible. The shape of the presented fundamental diagrams differs greatly between unidirectional and bidirectional movement and between the studies themselves, as has been widely recognised. In addition, they differ greatly in the measurement methods used to obtain the variables for the fundamental diagram.

Density and flow can be either directly measured [18] or calculated [17–19, 36, 38]. Among the subsequent studies, flow is calculated using density and speed and the flow equation, whereas the density calculation is based on [16, 17]. Some of the most recent studies show that the need to precisely define which portions of the respective quantities

J. Stat. Mech. (2026) 043401

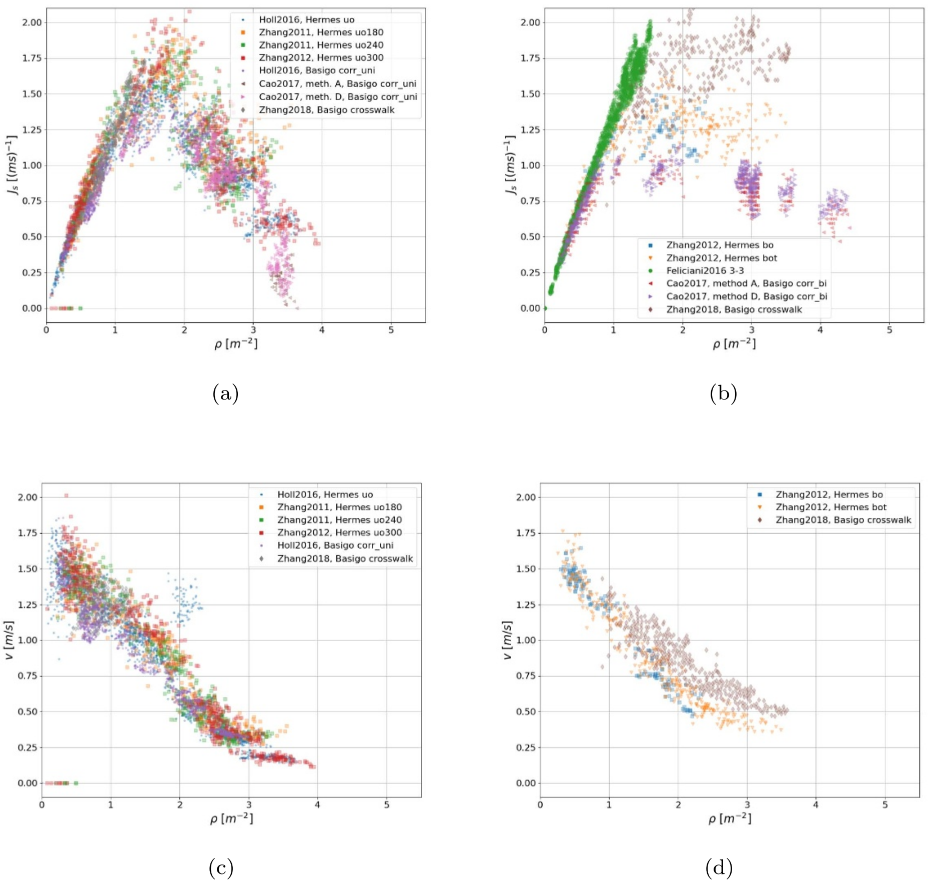

Figure 2. Fundamental diagrams for corridor experiments. (a), (c) Unidirectional streams. (b), (d) Bidirectional streams with two stationary lanes and bidirectional streams with multiple intersecting bands.

add to the flow or which sign has to be applied has been recognised. Most importantly, even under controlled conditions in the laboratory, the expected standstill at high densities does not appear. It is also noticeable that, unlike in experiments on single-file movement, all speed and flow values are positive. There may be various reasons for this. On the one hand, it may be that previous analyses of the experimental data were limited to the use of scalar quantities of velocity that are positive definite, such as speed as the magnitude of velocity. On the other hand, it may be that the number of test subjects for experiments under laboratory conditions was insufficient to cause a standstill. At least, the authors of this article have only succeeded in doing so in a single run, for a very short time, in experiments on unidirectional and bidirectional flows with 500 test subjects. These data are used here in section 3.2 to illustrate the problems of the analysis for fundamental diagrams of pedestrians.

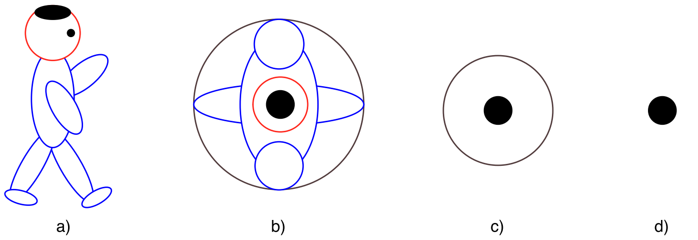

Figure 3. Simplification of the movement of a pedestrian for the state-of-the-art description of transport properties of crowds. The pedestrian from (a) side view and (b) top view. Although some approaches consider a volume exclusion, e.g. (c) by a circle, most analyses are based on (d) a point indicating the position of the head.

J. Stat. Mech. (2026) 043401

2.2. Variables

The movement of a pedestrian is performed by a three-dimensional body that continuously changes its shape by walking in steps.

To enable the analysis of many pedestrians moving in a crowd, the definitions of density, speed, and flow are based on a strong simplification. In general, the position of a body part, usually the head, is projected onto a two-dimensional space, and the head, with a diameter of 0.2 m, is represented by a point (figure 3).

For the definitions of variables describing transport properties of crowds, the movement of the human body of person i at time t, performed in a three-dimensional world, is abstracted by the movement of a point in two dimensions with position $\vec{r}_i(t)$ (see figure 4).

Microscopic representation

The movement of individual person i could be described by the position vector $\vec{x}_i(t)$ and the velocity $\vec{v}_i(t)$:

$$\vec{x}_i\,(t) = \begin{pmatrix} x_i\,(t) \\ y_i\,(t) \end{pmatrix} \quad \vec{v}_i\,(t) = \dot{\vec{x}}_i\,(t) = \begin{pmatrix} \dot{x}_i\,(t) \\ \dot{y}_i\,(t) \end{pmatrix}. \tag{1}$$

The position vector $\vec{x}_i(t)$ in time is the trajectory. Even for a single-file movement, the trajectory gained by tracking the head of a pedestrian is two-dimensional. The bipedal movement of the human body causes the upper body and head to sway orthogonally to the main direction of movement, which in figure 4(a) is the x direction. At high densities, pedestrians may come to a stop, standing in one place but shifting their balance from one leg to the other, causing their heads to move despite standing still. As a representation of such a situation by trajectories in the x–t plane shows, the head may move in the opposite direction to the main direction of movement x, which must lead to negative velocities. For pedestrian streams in wider corridors, the movement is two-dimensional, i.e. in the x–y plane (see figure 4(b)).

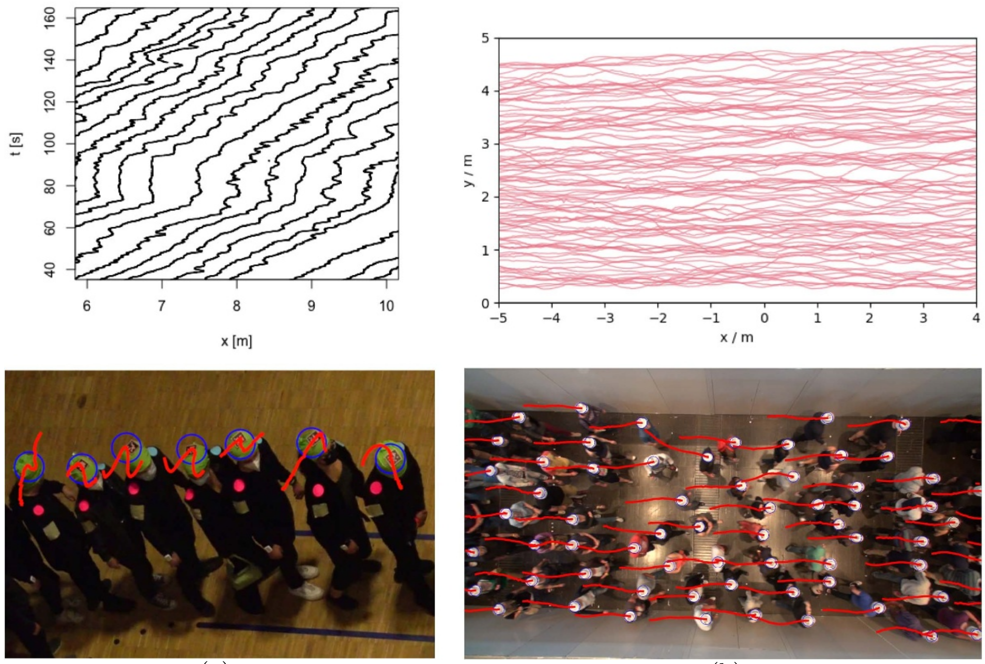

(a) (b)

Figure 4. (a) Example experiment on single-file movement. Top: individual trajectories, with x as the direction of movement. Bottom: snapshot of the experiment. (b) Example experiment on unidirectional flow in a corridor. Top: individual trajectories. Bottom: snapshot of the experiment. In both snapshots, blue circles represent the current head positions, and red lines indicate head trajectories over a time interval $[-1\,\mathrm{s}, 1\,\mathrm{s}]$ in (a) and $[-1\,\mathrm{s}, 0\,\mathrm{s}]$ in (b) from the current frame.

Two methods are used to define speed: the magnitude v_i of the velocity vector or the component of the velocity in the main direction of movement $\vec{n}_{\text{main}}$:

$$v_i\,(t) = \mid \vec{v}_i\,(t)\mid \quad \text{or} \quad v_{i,\text{main}}\,(t) = \vec{v}_i\,(t)\ \ \vec{n}_{\text{main}}. \tag{2}$$

Although position and velocity can be assigned to a single person, quantities such as distance and flow need to be related to at least a second person j.

To measure the flow, a cross section, e.g. a line l_0 at x_0, has to be introduced (see figure 5(a)). The time at which the pedestrians cross the line l_0 is $t_i(x_0) = t_{i,l_0}$. These times are sorted from the first to the last crossing to determine the time interval between two consecutive people crossing l_0, which is $\tau_{i,l_0} = t_{i-1}(x_0) - t_i(x_0)$. Following the above, an individual microscopic flow can be assigned to a person i by $J_{i,l_0} = (\tau_{i,l_0})^{-1}$.

The size of the area assigned to an individual person is A_i. The value A_i can be estimated either by the inverse of the macroscopic density or by the size of the Voronoi cell associated with pedestrian i [16].

J. Stat. Mech. (2026) 043401

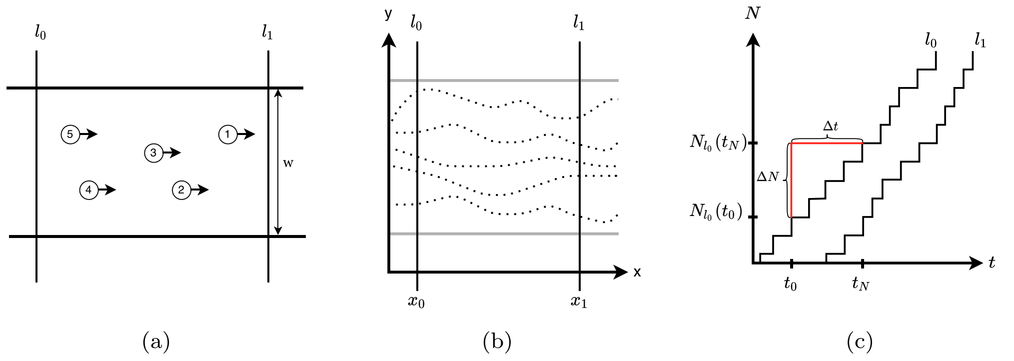

Figure 5. (a) Sketch of a corridor with width w in which five individuals walk from left to right between measuring lines l_0 and l_1. (b) Trajectories of individuals moving on the x–y plane in the x direction between l_0 at $x = x_0$ and l_1 at $x = x_1$. (c) $N-t$ diagram showing the cumulative count N of people having crossed l_0 and l_1 at time t.

Macroscopic representation

In physics and engineering, the classical way for a macroscopic description of pedestrian systems is based on mean values over time and space using trajectories, in other words, the Lagrangian specification of the system. In the following, we use the superscript c to index these variables. In a mathematical context, variables could also be based on an Euler specification of the system by fields. Later, the Voronoi decomposition is used to define these fields, and variables based on fields are indexed by the superscript v.

For mean values in time, the position is fixed at measurement line l_0, and movement is regarded within the time interval Δt. The start and end points of the time interval used for averaging are assigned to the crossing times of the first pedestrian t_{0,l_0} and the last pedestrian t_{N,l_0}, respectively. $N_{l_0,\Delta t}$ indicates the number of people who have crossed the measurement line l_0 within the time interval $]t_{0,l_0}, t_{N,l_0}]$ (see figure 5(c)). The flow is given by

$$J^{\mathrm{c}}_{l_0,\Delta t} = \frac{N_{l_0,\Delta t}}{\Delta t + \epsilon(t)}, \tag{3}$$

where ϵ considers that for a fixed magnitude of the time interval Δt, the time of crossing of the last person is not necessarily equal to the time of crossing of the first person plus the time interval selected for the measurement: $t_{N,l_0} \neq t_{0,l_0} + \Delta t$. For simplicity, $\Delta t + \varepsilon$ is denoted by Δt in the following. Figure 5(c) shows that introducing ϵ is necessary to consider the discreteness of crossings.

To assign a temporal mean value of the velocity to the macroscopic flow at l_0, individual velocities $\vec{v}_i(t_{i,l_0})$ at the time of the transition t_{i,l_0} over the measuring line are calculated and averaged. The mean velocity within the time interval Δt at line l_0 can be obtained by

$$\vec{v}_{l_0,\Delta t} = \frac{1}{N_{l_0,\Delta t}} \sum_{i=1}^{N_{l_0,\Delta t}} \vec{v}_i\left(t_{i,l_0}\right). \tag{4}$$

J. Stat. Mech. (2026) 043401

For mean values of speed over time, either the magnitude or the component of the main direction of movement (here, the direction orthogonal to the measurement line $\vec{n}_{l_0}$) is used:

$$v^{\mathrm{c}}_{l_0,\Delta t} = \frac{1}{N_{l_0,\Delta t}} \sum_{i=1}^{N_{l_0,\Delta t}} v_{i,l_0} \quad \text{or} \quad v^{\mathrm{c}}_{l_0,\Delta t,\perp} = \frac{1}{N_{l_0,\Delta t}} \sum_{i=1}^{N_{l_0,\Delta t}} v_{i,\perp}. \tag{5}$$

For the calculation of mean values of the velocity in space, the measurements are based on an area A, whereas the time is fixed at t_0, e.g. between both measurement lines l_0 and l_1 in figure 5(b). The mean velocity $\vec{v}_{t_0,A}$ within the measurement area $A = \Delta x \cdot w$ with $\Delta x = x_1 - x_0$, where w is the width of the corridor in the y direction, can be obtained by

$$\vec{v}_{A,t_0} = \frac{1}{N_{A,t_0}} \sum_{i=1}^{N_{A,t_0}} \vec{v}_i\,(t_0)\,, \tag{6}$$

where N_{A,t_0} is the number of pedestrians inside A at time t_0. Again, it should be differentiated between mean values of the magnitude v^{c}_{A,t_0} and the velocity component in the main direction of movement $v^{\mathrm{c}}_{A,t_0,\perp}$. Classically, the density ρ is defined as

$$\rho^{\mathrm{c}}_A\,(t) = \frac{N_A\,(t)}{A}, \tag{7}$$

where $N_A(t)$ is the number of pedestrians inside A at time t. Unfortunately, the size of the objects (here, the size of the pedestrians) is of the same order of magnitude as the size of A, leading to high fluctuations of the classical density. To overcome this problem, a Voronoi decomposition of the space can be used (see [16]). The positions $\vec{x}_i(t)$ of pedestrians $i = 1,\ldots,N$ are used to construct a scalar density field $\boldsymbol{\rho}(\vec{x},t)$ by decomposing the space into Voronoi cells $A_i(t) = A_i(\vec{x}_i(t))$ based on the positions of the pedestrians $\vec{x}_i(t)$. Scalar and vector fields are written in bold letters in the following. The resulting field is given by

$$\boldsymbol{\rho}\,(\vec{x},t) = \sum_i \boldsymbol{\rho}_i\,(\vec{x},t) \;\text{ with }\; \boldsymbol{\rho}_i\,(\vec{x},t) = \left\{ \begin{array}{ll} 1/A_i\,(t): & \vec{x} \in A_i\,(t) \\ 0: & \text{otherwise} \end{array} \right\}. \tag{8}$$

The Voronoi decomposition is only one possible method to construct a density field. Other options include using a Gaussian distribution [39]. We prefer the Voronoi decomposition because it is parameter-free and allows easy consideration of boundaries. The density in a measurement area A at a certain time t is then

$$\rho^{\mathrm{v}}_A\,(t) = \frac{1}{A} \int_A \boldsymbol{\rho}\,(\vec{x},t)\; \mathrm{d}\vec{x}. \tag{9}$$

Using distribution functions to define a density field smoothes the density measurements in space and time. It allows defining an individual density $\rho_i(t) = \rho^{\mathrm{v}}_{A_i(t)} = 1/A_i(t)$ or even measurement areas smaller than the size of a single pedestrian.

Although Edie's framework allows, in principle, the use of very small space–time regions, this option has limited practical value for trajectory-based pedestrian data. Owing to the discrete and sparse nature of such data, many of these regions remain empty, which leads to undefined or discontinuous quantities. Hence, Edie's approach cannot provide the continuous local fields required to maintain consistency with the continuity equation.

3. Continuity equation with Voronoi-based fields

The microscopic and macroscopic definitions of the quantities in the previous section form the basis for measurements of the fundamental diagram and the application of the flow equation. Various aspects point to fundamental problems in the use of the variables with these definitions. An examination of the type of mean value that is linked already reveals inconsistencies. For example, $J(\rho)$ relates $J_{l_0,\Delta t}$ to ρ_{A,t_0} and thus combines the mean value over time with the mean value over space. Thus, the quantities relate to different areas in phase space. The same inconsistency appears in the flow equation $J = \rho v w$. The inconsistencies that may arise when converting fundamental diagrams using the flow equation are shown in [23]. However, even if mean values over time and space are used separately and not mixed, the discussion in section 1 shows that, to date, fundamental diagrams are not in conformance with plausible expectations. In relation to particle number conservation, which is manifested by the continuity equation, the following problems of the flow equation arise. First, classical measurements of the mean values are not uniformly definable with respect to the measurement area in space and time. Second, the formulation is not sufficiently precise for the calculation of v. The velocity of individual pedestrians $\vec{v}_i$ is a vector in a two-dimensional system, including information about the direction of the movement, and a definition of the scalar mean value $v = f(\vec{v}_1(t), \ldots, \vec{v}_N(t))$ is generally not provided.

There are several reasons why this has been overlooked until now. First, historical data are associated with very rough estimates of speed, flow, and density, which make a precise definition of v seemingly unnecessary. Second, there are currently little experimental data that capture a standstill. Third, research has been strongly oriented toward vehicular traffic, which is treated as a quasi-one-dimensional system due to traffic lanes. By contrast, the capture of individual two-dimensional trajectories at a time discreteness of about one-tenth of a second achieves a level of accuracy that may become relevant, particularly for high densities and inhomogeneous systems. Moreover, the trajectories used represent head positions, and because pedestrian head movement can involve large fluctuations and velocities in the opposite direction as the walking direction, additional problems arise.

3.1. Continuity equation

In the following, the field formulation of the continuity equation serves as the starting point for enabling spatiotemporally consistent measurement of the scalars j, ρ, and v. To link this formulation with the measurement of discrete trajectories of individual pedestrians $\vec{x}_i(t)$, the Voronoi decomposition $A_i(\vec{x}_i(t))$ is used to construct the fields.

First, the flow equation is formulated for a typical measurement scenario:

$$\frac{\mathrm{d}N_A}{\mathrm{d}t} + \oint_l \vec{\boldsymbol{j}}\,(\vec{x},t)\cdot \mathrm{d}\vec{l} = 0, \tag{10}$$

where N_A is the number of all pedestrians in the area A, l is a line enclosing the area, and $\vec{j}$ is the flow field of N_A. The flow field is connected with the velocity field $\vec{u}$ by

$$\vec{\boldsymbol{j}}\,(\vec{x},t) = \boldsymbol{\rho}\,(\vec{x},t)\,\vec{\boldsymbol{v}}\,(\vec{x},t)\,. \tag{11}$$

Note that this is an integral of the flow field along a line. When the flow field is directed parallel to the line, the flow through the line is zero. When it flows perpendicular to the line, it is maximum. Only the component of the flow vector, which is perpendicular to the line $j^{\perp} = \vec{\boldsymbol{j}}\cdot\vec{n}$, is contributing to the change in the number of pedestrians in A, with $\vec{n}$ being the normal vector to the line.

In the example presented in figure 5(b), the measurement area $A = w\cdot(x_1 - x_0)$ is enclosed by line l, consisting of two lines in the x direction along the corridor walls between l_0 and l_1, and two lines in the y direction along l_0 and l_1, each with a length of w. Because there is no movement through the walls of the corridor, the flow only needs to be measured along the measurement lines l_0 and l_1. Then, the continuity equation is

$$\frac{\mathrm{d}N_A}{\mathrm{d}t} = \int_{l_0} \vec{\boldsymbol{j}}\cdot \mathrm{d}\vec{l} + \int_{l_1} \vec{\boldsymbol{j}}\cdot \mathrm{d}\vec{l} = \int_{l_0} \boldsymbol{\rho}\vec{\boldsymbol{v}}\cdot\vec{n}\cdot \mathrm{d}y + \int_{l_1} \boldsymbol{\rho}\vec{\boldsymbol{v}}\cdot\vec{n}\cdot \mathrm{d}y, \tag{12}$$

with $\vec{n}$ pointing towards the inside of the measurement area. For the flow J as the mean value within time interval $\Delta t = [t_0, t_N]$ (see equation (3)), the continuity equation is

$$\frac{N_{t_N,A} - N_{t_0,A}}{t_N - t_0} = J_{l_0,\Delta t} + J_{l_1,\Delta t}. \tag{13}$$

Using equation (11), the flow equation for a certain point in time at line l_0 at x_0 is

$$J_{l_0}(t) = \int_{y_0}^{y_1} \vec{\boldsymbol{j}}\,(x_0,y,t)\;\vec{n}_{l_0}\;\mathrm{d}y = \int_{y_0}^{y_1} \boldsymbol{\rho}\,(x_0,y,t)\;\vec{\boldsymbol{v}}\,(x_0,y,t)\;\vec{n}_{l_0}\;\mathrm{d}y. \tag{14}$$

The macroscopic flow during the time interval Δt is given by

$$\begin{aligned} J_{l_0,\Delta t} &= \frac{1}{\Delta t}\int_{t_0}^{t_N}\int_{y_0}^{y_1} \vec{\boldsymbol{j}}\,(x_0,y,t)\;\vec{n}_{l_0}\;\mathrm{d}y\;\mathrm{d}t \\ &= \frac{1}{\Delta t}\int_{t_0}^{t_N}\int_{y_0}^{y_1} \boldsymbol{\rho}\,(x_0,y,t)\;\vec{\boldsymbol{v}}\,(x_0,y,t)\;\vec{n}_{l_0}\;\mathrm{d}y\;\mathrm{d}t. \end{aligned} \tag{15}$$

Comparing equation (15) with the classical flow equation $J = \rho\; v\; w$ reveals the following ambiguities.

First, the classical flow equation itself does not specify how the value of the scalar v is calculated from velocity, which is a vector. This means that there is no clear rule for converting velocity into speed. In particular, for the oscillating trajectories of the heads of pedestrians, the calculation of the magnitude of the velocity leads to an overestimation of the fraction of the velocity that contributes to the flow or the throughput. Movements of the head opposite to the main direction of the motion of the stream, e.g. when pedestrians are standing still, must be considered by a negative contribution to the velocity and flow. For the calculation of real throughput in the case of pedestrian streams with different main movement directions (bidirectional or multidirectional streams), it is essential to distinguish negative contributions due to head oscillations opposite to the main direction with positive contributions in the main direction from the opposing stream.

Second, the density ρ is usually measured as the mean value over a two-dimensional measurement area. Only in cases in which the density is homogeneous in space is it a reasonable approximation of the density at a measurement line. In particular, at high densities in which congestion leads to density waves moving through the measurement area, the difference between a line density and an area density can be significant.

Third, multiplication by the length of the measurement line w implies that the product of density and velocity along the measurement line is constant, which is related to the concept of specific flow. However, density, velocity, or their product may also be inhomogeneous along the measurement line, which can be accompanied by a violation of the concept of specific flow.

Fourth, it should be noted that, in general, the mean value of the product of density and velocity is not equal to the product of their mean values. In fact, one can write

$$\langle \rho v \rangle = \langle \rho \rangle \langle v \rangle + \mathrm{cov}(\rho, v), \tag{16}$$

where $\langle \cdot \rangle$ denotes the integral along the measurement line, and $\mathrm{cov}(\rho, v)$ is the covariance with respect to this measure, which may be positive or negative. Neglecting the covariance term corresponds to a mean-field approximation.

3.2. Flow equation by Voronoi fields for unidirectional streams

The following methodology is proposed to handle the problems outlined above and connect the trajectories of pedestrians with the continuity equation. First, a set of trajectories of M persons $x_1(t), \ldots, x_M(t)$ is used to calculate the Voronoi decomposition and to introduce a density field $\boldsymbol{\rho}$ and a velocity field $\vec{\boldsymbol{v}}$:

$$\boldsymbol{\rho}(\vec{x}, t) = \sum_{i=1}^{M} \boldsymbol{\rho}_i(\vec{x}, t) \text{ with } \boldsymbol{\rho}_i(\vec{x}, t) = \left\{ \begin{array}{ll} 1/A_i(t): & \vec{x} \in A_i(t) \\ 0: & \text{otherwise} \end{array} \right\} \tag{17}$$

$$\vec{\boldsymbol{v}}(\vec{x}, t) = \sum_{i=1}^{M} \vec{\boldsymbol{v}}_i(\vec{x}, t) \text{ with } \vec{\boldsymbol{v}}_i(\vec{x}, t) = \left\{ \begin{array}{ll} \vec{v}_i(t): & \vec{x} \in A_i(t) \\ 0: & \text{otherwise} \end{array} \right\}. \tag{18}$$

With this definition of fields, a person's contribution is limited to their own Voronoi cell. Outside the cell, the contribution is 0. To define the fields, the contributions of individual cells can simply be summed up and by definition without overlapping. These fields are used in combination with equation (14) to define the flow field $\vec{\boldsymbol{j}}(\vec{x}, t)$ following the continuity equation:

$$J^{\mathrm{v}}_{l_0}(t) = \int_{y_0}^{y_1} \vec{\boldsymbol{j}}(x_0,y,t)\ \vec{n}_{l_0}\ \mathrm{d}y \tag{19}$$

$$= \int_{y_0}^{y_1} \boldsymbol{\rho}(x_0,y,t)\ \vec{\boldsymbol{v}}(x_0,y,t)\ \vec{n}_{l_0}\ \mathrm{d}y \tag{20}$$

$$= \int_{y_0}^{y_1} \left(\sum_i \boldsymbol{\rho}_i(x_0,y,t)\right) \left(\sum_j \vec{\boldsymbol{v}}_j(x_0,y,t)\ \vec{n}_{l_0}\right)\ \mathrm{d}y. \tag{21}$$

All terms in the product of the sums with $i \neq j$ are zero by definition of the fields $\boldsymbol{\rho}(\vec{x},t)$ and $\vec{\boldsymbol{v}}(\vec{x},t)$. In addition, within a Voronoi cell $A_i(t)$, the fields are constant; thus, the integral over the measurement line l_0 can be replaced by the following sum:

$$J^{\mathrm{v}}_{l_0}(t) = \int_{y_0}^{y_1} \left(\sum_i \boldsymbol{\rho}_i(x_0,y,t)\ \vec{\boldsymbol{v}}_i(x_0,y,t)\ \vec{n}_{l_0}\right)\ \mathrm{d}y \tag{22}$$

$$= \sum_{\{i|A_i(t)\in l_0\}} \frac{\vec{v}_i(t)\ \vec{n}_{l_0}}{A_i(t)}\ w_{i,l_0}(t) \tag{23}$$

$$= \sum_{\{i|A_i(t)\in l_0\}} \rho_i(t)\ v_i(t)^{\perp_{l_0}}\ w_{i,l_0}(t), \tag{24}$$

where $w_{i,l_0}(t)$ is the length of the intersection between measurement line l_0 and the Voronoi cell $A_i(t)$ (see figure 6). This is consistent with the following definition of a flow field based on Voronoi decomposition:

$$\vec{\boldsymbol{j}}(\vec{x},t) = \sum_i \vec{\boldsymbol{j}}_i(\vec{x},t)\ \text{ with } \vec{\boldsymbol{j}}_i(\vec{x},t) = \left\{ \begin{array}{ll} \frac{\vec{v}_i(t)}{A_i(t)}: & \vec{x}\in A_i(t) \\ 0: & \text{otherwise} \end{array} \right\}. \tag{25}$$

To compare the field definition by Voronoi decomposition with classical measurements of speed and density, see equations (4) and (7), in which integration is performed over the measurement lines and a mean value is calculated by dividing by the length w of the measurement line l_0 :

$$v^{\mathrm{v}}_{l_0}(t) = \frac{1}{w}\int_{y_0}^{y_1} \vec{\boldsymbol{v}}(\vec{x},t)\vec{n}_{l_0}\ \mathrm{d}y = \sum_{\{i|A_i(t)\in l_0\}} \vec{v}_i(t)\vec{n}_{l_0}\frac{w_{i,l_0}(t)}{w} \tag{26}$$

$$\rho^{\mathrm{v}}_{l_0}(t) = \frac{1}{w}\int_{y_0}^{y_1} \boldsymbol{\rho}(\vec{x},t)\ \mathrm{d}y = \sum_{\{i|A_i(t)\in l_0\}} \frac{1}{A_i(t)}\frac{w_{i,l_0}(t)}{w} \tag{27}$$

$$J^{\mathrm{v}}_{\mathrm{s},l_0}(t) = \frac{1}{w}\int_{y_0}^{y_1} \vec{\boldsymbol{j}}(\vec{x},t)\vec{n}_{l_0}\ \mathrm{d}y = \sum_{\{i|A_i(t)\in l_0\}} \frac{\vec{v}_i(t)\vec{n}_{l_0}}{A_i(t)}\frac{w_{i,l_0}(t)}{w}. \tag{28}$$

A comparison of the mean density, velocity, and specific flow shows that integrating the weights results in a linear factor in each case. This emphasises the importance of

J. Stat. Mech. (2026) 043401

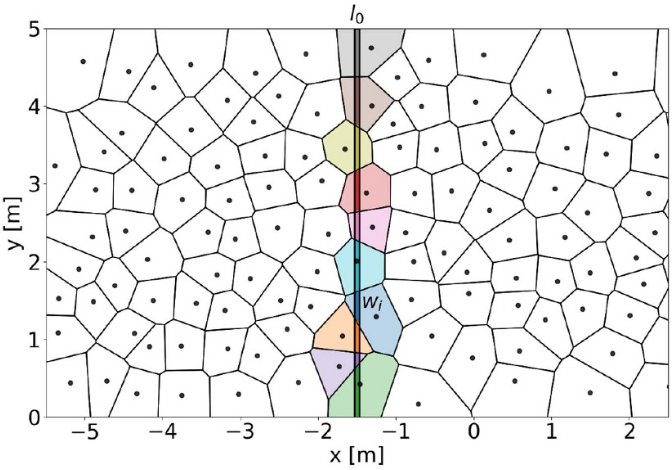

Figure 6. Voronoi decomposition for head positions marked by black dots. Voronoi cells intersecting with the measurement line l_0 are indicated by face colours, whereas the actual intersection w_i with the line is indicated by brighter colours.

the correct application of mean values (see equation (16)). With these fields, the flow equation at every point in time along the measurement line l_0 is

$$J_{l_0}^{\mathrm{v}}(t) = \int_{y_0}^{y_1} \vec{\boldsymbol{j}}(\vec{x},t)\,\vec{n}_{l_0}\,\mathrm{d}y = \sum_{\{i|A_i(t)\in l_0\}} \frac{\vec{v}_i(t)\,\vec{n}_{l_0}}{A_i(t)}\,w_{i,l_0}(t)$$
$$= \sum_{\{i|A_i(t)\in l_0\}} \rho_i(t)\ v_i(t)^{\perp_{l_0}}\ w_{i,l_0}(t). \tag{29}$$

The following classical measurement methods based on the trajectories of particles are compared with the measurements based on the fields constructed via Voronoi decomposition. Classical measurements are given the superscript c, whereas field measurements based on Voronoi decomposition are denoted by the superscript v. For this comparison, we use data from experiments conducted under laboratory conditions. In general, video recordings with a frame rate of, e.g. 25 frames s^{-1}, are used. This leads to trajectories discrete in time t_k, where $k = 1,\ldots,M$, but continuous in space $\vec{x}_i(t_k)$. A measurement of flow J as a mean value over the time interval $\Delta t = t_N - t_0$ at the line l_0 according to equation (15) is

$$J_{l_0,\Delta t}^{\mathrm{v}} = \frac{1}{M}\sum_{k=1}^{M}\left(\sum_{\{i|A_i(t_k)\in l_0\}} \frac{\vec{v}_i(t_k)\,\vec{n}_{l_0}}{A_i(t_k)} w_{i,l_0}(t_k)\right) \tag{30}$$

where $t_0 = t_{k=1}$ and $t_N = t_{k=M}$.

At high densities, several persons can walk side by side across l_0, and the time interval τ_{i,l_0} between two successive crossings can be rather small. When calculating the flow according to $J_{l_0,\Delta t}^{\mathrm{c}} = \frac{N}{t_N - t_0}$, it is therefore possible that more than one pedestrian crosses l_0 between two consecutive frames t_k and t_{k+1}, e.g. $t_k < t_i < t_{i+1} < t_{k+1}$. This

J. Stat. Mech. (2026) 043401

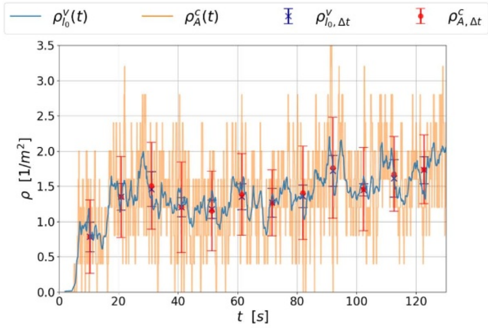

(a)

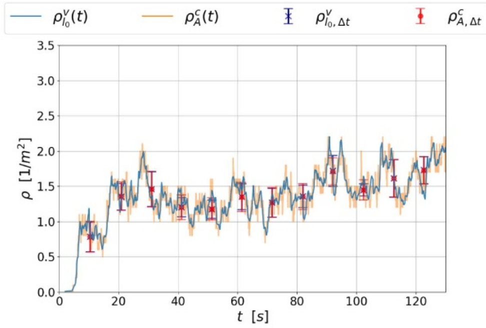

(b)

Figure 7. Density–time series for the uni_corr_500_03 experiment. Comparison between the line density $\rho^{\mathrm{v}}_{l_0}(t)$ (equation (27)) and the classical density $\rho^{\mathrm{c}}_{A}(t)$ (equation (7)). Their mean values within time intervals $\Delta t = 10\,\mathrm{s}$ are $\rho^{\mathrm{v}}_{l_0,\Delta t}$ and $\rho^{\mathrm{c}}_{A,\Delta t}$, respectively. For the classical density, the measurement area around l_0 has a width of (a) $\Delta x = 0.5\,\mathrm{m}$ and (b) $\Delta x = 2\,\mathrm{m}$.

requires an adequate interpolation of the trajectories between t_k and t_{k+1}. The velocity of an individual at t_k is calculated by

$$\vec{v}_i\left(t_k\right) = \frac{\vec{x}_i\left(t_{k+n}\right) - \vec{x}_i\left(t_{k-n}\right)}{t_{k+n} - t_{k-n}}. \tag{31}$$

For the following measurement, we use $n = 10$.

As examples for unidirectional flow, we use the datasets of the uni_corr_500 experiments (https://doi.org/10.34735/ped.2013.6) that were acquired in a corridor with $w = 5\,\mathrm{m}$ width in the framework of the BASIGO project. The two subexperiments that we examine in more detail are uni_corr_500_03, in which the flow is close to its maximum, and uni_corr_500_10, which has the highest density, i.e. the flow is decreased. In figures 7 and 8, we compare the line density $\rho^{\mathrm{v}}_{l_0}(t)$ with the classical density $\rho^{\mathrm{c}}_{A}(t)$ measured within a narrow and wide measurement area. In the case of the uni_corr_500_03 experiment, the mean values $\rho^{\mathrm{v}}_{l_0,\Delta t}$ and $\rho^{\mathrm{c}}_{A,\Delta t}$ within a 10 s time interval are in good correspondence within the error limits. However, for the uni_corr_500_10 experiment, there are some deviations between the classical and field measurements of density, indicating the relevance of spatial inhomogeneities under crowded conditions.

A comparison between the line speed $v^{\mathrm{v}}_{l_0}(t)$ and the classical crossing speed $v^{\mathrm{c}}_{i,l_0,\perp}(t)$ is shown in figure 9. Again, both methods correspond well to the uni_corr_500_03 experiment. However, in the uni_corr_500_10 experiment, there are clear deviations. This can be explained as follows. When using the classical crossing speed $v^{\mathrm{c}}_{i,l_0,\perp}(t)$, moving pedestrians are taken into account while crossing the line. Pedestrians in standstill shortly in front or behind the line are not considered. In the measurements of the line speed based on field $v^{\mathrm{v}}_{l_0}(t)$, standing pedestrians whose Voronoi cell intersects the line contribute to the integral. This is exactly the difference that can be seen in figure 9(b).

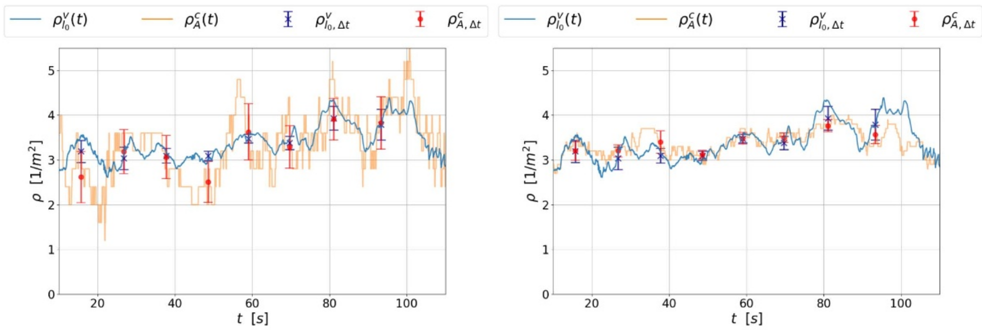

(a) (b)

Figure 8. Density–time series for the uni_corr_500_10 experiment. Comparison between the line density $\rho^{\mathrm{v}}_{l_0}(t)$ (equation (27)) and the classical density $\rho^{\mathrm{c}}_{A}(t)$ (equation (7)). Their mean values within time intervals $\Delta t = 10\,\mathrm{s}$ are $\rho^{\mathrm{v}}_{l_0,\Delta t}$ and $\rho^{\mathrm{c}}_{A,\Delta t}$, respectively. For the classical density, the measurement area around l_0 has a thickness of (a) $\Delta x = 0.5\,\mathrm{m}$ and (b) $\Delta x = 2\,\mathrm{m}$.

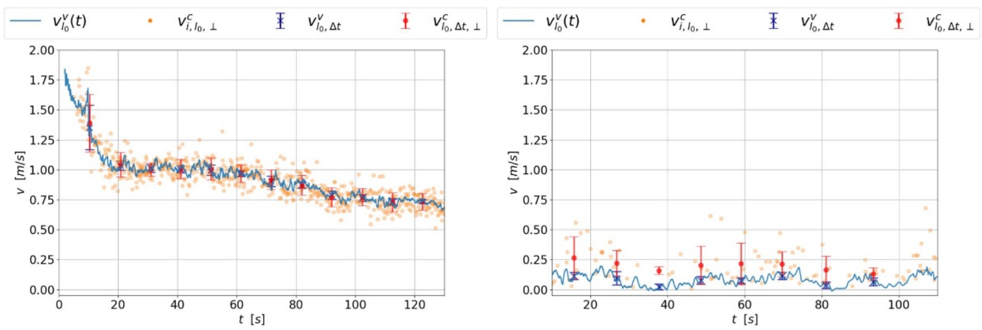

(a) (b)

Figure 9. Speed–time series for the (a) uni_corr_500_03 and (b) uni_corr_500_10 experiments. Comparison between $v^{\mathrm{v}}_{l_0}(t)$ (equation (26)) and the classical individual perpendicular crossing velocity $v^{\mathrm{c}}_{i,l_0,\perp}$. Their mean values within time intervals $\Delta t = 10\,\mathrm{s}$ are $v^{\mathrm{v}}_{l_0,\Delta t}$ and $v^{\mathrm{c}}_{l_0,\Delta t,\perp}$ (equation (5)), respectively.

Figure 10 compares classical flow measurements according to equation (3) with the new method (equation (30)). The comparison shows good agreement and the expected alignment with negative flow values.

Finally, the fundamental diagram in figure 11 provides a general overview of the comparison between the proposed measurement methods of density $\rho^{\mathrm{v}}_{l_0}$ along a line and the specific flow $J^{\mathrm{v}}_{\mathrm{s},l_0,\Delta t}$ with the classical measurement methods for density ρ^{c}_{A} within a measurement area and the specific flow $J^{\mathrm{c}}_{\mathrm{s},l_0,\Delta t}$. The general course of the fundamental diagrams is similar. Deviations can mostly be seen in the high-density regime, which results from differences in the determination of density and speed.

To summarise, we have demonstrated a method that makes it possible to calculate all three variables (density, velocity, and flow) along a line, thus avoiding the mixing of mean values in space and time.

J. Stat. Mech. (2026) 043401

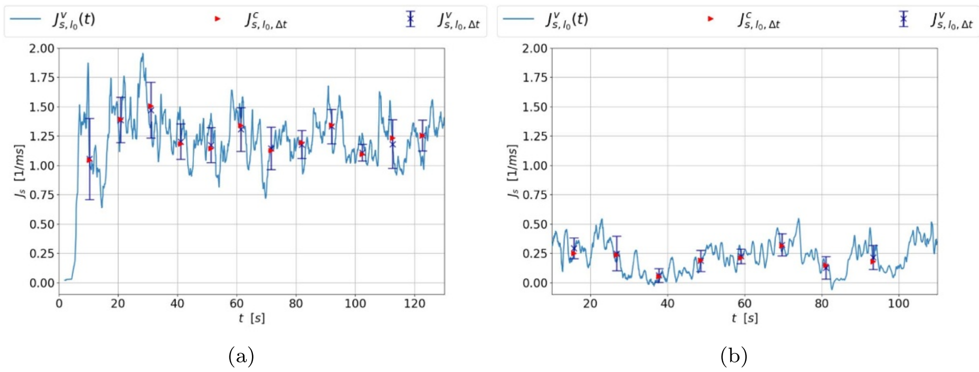

Figure 10. Flow–time series for the (a) uni_corr_500_03 and (b) uni_corr_500_10 experiments. Comparison between the specific flow $J^{\mathrm{v}}_{\mathrm{s},l_0}(t)$ (equation (28)) with mean value $J^{\mathrm{v}}_{\mathrm{s},l_0,\Delta t}$ and the classical specific flow $J^{\mathrm{c}}_{\mathrm{s},l_0,\Delta t}$ measured after equation (3) with $\Delta t = 10\,\mathrm{s}$.

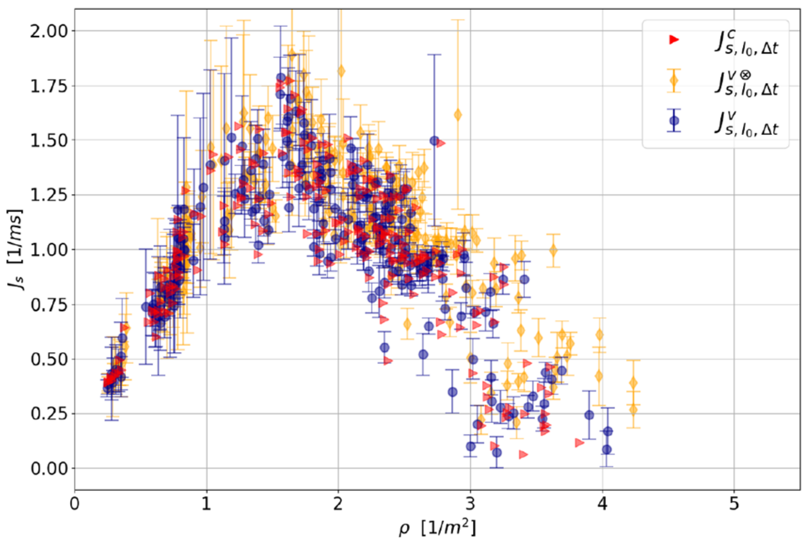

Figure 11. Fundamental diagram for unidirectional flow uni_corr_500 experiments averaged within time intervals of $\Delta t = 5\,\mathrm{s}$. Comparison between the new method in blue (specific flow $J^{\mathrm{v}}_{\mathrm{s},l_0,\Delta t}$ (equation (28)) using line density $\rho^{\mathrm{v}}_{l_0,\Delta t}$ (equation (27))) with classical measurements in red (specific flow $J^{\mathrm{c}}_{\mathrm{s},l_0,\Delta t}$ (equation (3)) and density $\rho^{\mathrm{c}}_{A,\Delta t}$ (equation (7)) within a measurement area of width $\Delta x = 2\,\mathrm{m}$) and a simplified measurement in yellow (with specific flow $J^{\mathrm{v}\otimes}_{\mathrm{s},l_0,\Delta t}$ (equation (48)) and density $\rho^{\mathrm{v}\otimes}_{l_0,\Delta t}$ (equation (45)).

3.3. Flow equation by Voronoi fields for bidirectional or multidirectional streams

The equations developed in the previous subsection also ensure conformity with the continuity equation for bidirectional and multidirectional streams. However, we must consider the two possible main movement directions that pedestrians may have when

J. Stat. Mech. (2026) 043401

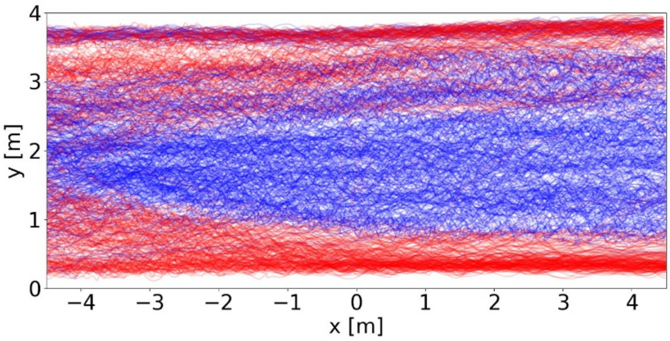

(a)

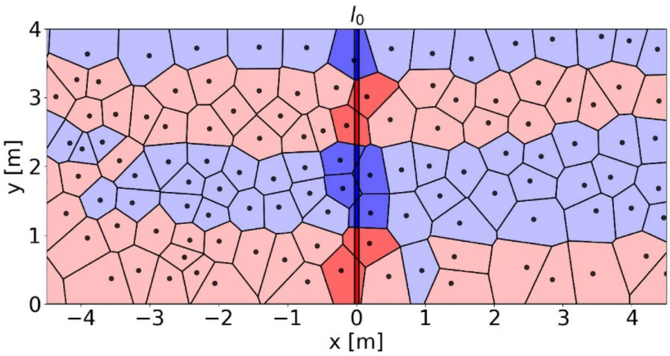

(b)

Figure 12. Exemplary experimental dataset for bidirectional flow in a corridor. (a) Individual head trajectories and (b) Voronoi decomposition. Red and blue indicate the direction of the opposing main movement. In (b), the Voronoi cells intersecting with measurement line l_0 are indicated by a brighter colour.

crossing a line. The calculation of the flow $J^{\mathrm{v}}_{l_0}(t)$ uses the velocity components perpendicular to the measurement line l_0, including the sign to explicitly allow the perpendicular speed to be negative. This is done to account for crossings in the opposite direction of the desired main movement direction, treated as a negative contribution to the measured flow. Although this is right for the conservation of particle numbers in the control volume, it leads to an inappropriate description of the performance of the corridor cross section (see equation (3)). To define the performance of a system for multidirectional flows at line l_0, a distinction must be made between pedestrians with different main movement directions.

For bidirectional streams, two species (I and II) are introduced according to the two possible main movement directions concerning the measurement line l_0 (see figure 12). For both species, the fields are defined separately. However, to still consider that these

J. Stat. Mech. (2026) 043401

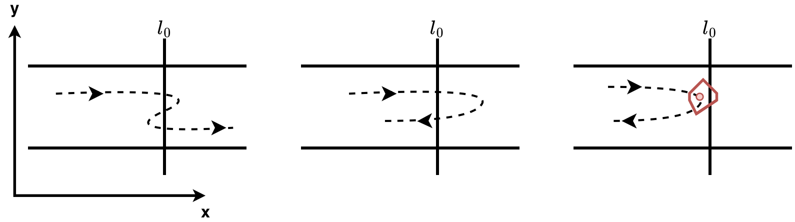

Figure 13. Examples of trajectories and options for assigning trajectories to a species.

streams share the same available space, the definitions are based on a unique Voronoi decomposition considering the positions $\vec{r}_i$ of all pedestrians i.

In figure 13, different possibilities of crossings are sketched. In the first sketch, the pedestrian has multiple crossings of the measurement line but successfully moves to the main direction of motion (here, the positive x direction). The middle sketch shows an example in which the pedestrian tries to move in the positive x direction but does not succeed and walks back into the negative x direction. The last sketch on the right shows an example in which the pedestrian tries to move in the positive x direction, but the trajectory $\vec{r}(t)$ never crosses the measurement line l_0, whereas the Voronoi cell constructed using its position $\vec{r}_i(t)$ crosses the line l_0.

For each pedestrian i, the intended direction of movement was determined by the direction from which they approached the measurement line. More specifically, for each person, we recorded on which side the measurement line was first touched by their Voronoi cell. The intended direction of movement is then defined as the direction from which the person will cross the line. For example, if the first contact with the measurement line is from the left, the intended direction of movement is defined as from left to right.

This definition ensures that every pedestrian i with $A_i(t) \in l_0$ is associated with at least one species. We introduce a factor m as the direction of the orthogonal velocity at the time $t_{i,l_0} = \min(t|A_i(t) \in l_0)$, when the Voronoi cell $A_i(t)$ of pedestrian i touches the measurement line l_0 the first time by

$$m = \operatorname{sign}\left(\vec{n} \cdot \vec{v}\left(t_{i,l_0}\right)\right) \tag{32}$$

where $\vec{n}$ is the unit vector orthogonal to l_0.

The separation of the two species (I and II) is made according to the sign of m:

$$\mathrm{I} = \{i\,|m = 1\} \text{ and } \mathrm{II} = \{i\,|m = -1\} \tag{33}$$

which means that the main movement direction of all pedestrians belonging to species I is in the same direction as $\vec{n}$. In contrast, the main movement direction of all pedestrians of species II is opposite to $\vec{n}$.

The intended main direction of movement, and thus the assignment to species I or II, remains unchanged even if a person changes their mind and turns around or if there are multiple crossings of the measuring line. In figure 13, different possibilities of crossings

https://doi.org/10.1088/1742-5468/ae458a

are sketched. By the definition given above, all three examples shown in figure 13 are assigned to species I. In the first sketch, the pedestrian has multiple crossings of the measurement line but successfully moves to the main direction of motion (here, in the positive x direction). The middle sketch shows an example in which the pedestrian tries to move in the positive x direction but does not succeed and instead walks back into the negative x direction. The last sketch on the right shows an example in which the pedestrian tries to move in the positive x direction. The trajectory $\vec{r}(t)$ never crosses the measurement line l_0, whereas the Voronoi cell constructed using its position $\vec{r}_i(t)$ crosses the line l_0.

The separate density field $\boldsymbol{\rho}^{\mathrm{S}}$, velocity field $\vec{\boldsymbol{v}}^{\mathrm{S}}$, and flow field $\vec{\boldsymbol{j}}^{\mathrm{S}}$ for both species with $S = \mathrm{I}$ and $S = \mathrm{II}$ are

$$\boldsymbol{\rho}^{\mathrm{S}}(\vec{x},t) = \sum_i \boldsymbol{\rho}_i(\vec{x},t) \text{ with } \boldsymbol{\rho}_i(\vec{x},t) = \left\{ \begin{array}{ll} 1/|A_i(t)|: & \vec{x} \in A_i(t) \wedge i \in S \\ 0: & \text{otherwise} \end{array} \right\} \tag{34}$$

$$\vec{\boldsymbol{v}}^{\mathrm{S}}(\vec{x},t) = \sum_i \vec{\boldsymbol{v}}_i(\vec{x},t) \text{ with } \vec{\boldsymbol{v}}_i(\vec{x},t) = \left\{ \begin{array}{ll} m \cdot \vec{v}_i(t): & \vec{x} \in A_i(t) \wedge i \in S \\ 0: & \text{otherwise} \end{array} \right\} \tag{35}$$

$$\vec{\boldsymbol{j}}^{\mathrm{S}}(\vec{x},t) = \sum_i \vec{\boldsymbol{j}}_i(\vec{x},t) \text{ with } \vec{\boldsymbol{j}}_i(\vec{x},t) = \left\{ \begin{array}{ll} \frac{m \cdot \vec{v}_i(t)}{A_i(t)}: & \vec{x} \in A_i(t) \wedge i \in S \\ 0: & \text{otherwise} \end{array} \right\}. \tag{36}$$

This definition allows a separate analysis of the streams in consistency with the continuity equation. To obtain the combined fields, the density and velocity fields of all pedestrians are added :

$$\boldsymbol{\rho}(\vec{x},t) = \boldsymbol{\rho}^{\mathrm{I}}(\vec{x},t) + \boldsymbol{\rho}^{\mathrm{II}}(\vec{x},t) \tag{37}$$

$$\vec{\boldsymbol{v}}(\vec{x},t) = \vec{\boldsymbol{v}}^{\mathrm{I}}(\vec{x},t) + \vec{\boldsymbol{v}}^{\mathrm{II}}(\vec{x},t). \tag{38}$$

Owing to $\boldsymbol{\rho}^{\mathrm{I}}(\vec{x},t) \cdot \vec{\boldsymbol{v}}^{\mathrm{II}}(\vec{x},t) = 0$ and $\boldsymbol{\rho}^{\mathrm{II}}(\vec{x},t) \cdot \vec{\boldsymbol{v}}^{\mathrm{I}}(\vec{x},t) = 0$, the flow fields of the two species can also be added:

$$\vec{\boldsymbol{j}}(\vec{x},t) = \vec{\boldsymbol{j}}^{\mathrm{I}}(\vec{x},t) + \vec{\boldsymbol{j}}^{\mathrm{II}}(\vec{x},t). \tag{39}$$

As an example of bidirectional flow, the datasets of the bi_corr_400 experiments (https://doi.org/10.34735/ped.2013.5) with a corridor width of 4 m are used, acquired within the framework of the BASIGO project. In figure 14, the exemplary time series of speed are shown. Figure 14(a) shows the run in which the flow is close to its maximum. Figure 14(b) shows the speed of the experimental run with the highest density. The comparison between the proposed speed measurement method at the line $v^{\mathrm{v}}_{l_0}$ with the classical vertical velocity at the time of the crossing $v^{\mathrm{c}}_{i,l_0,\perp}$ is similar to that of the unidirectional experiments. The velocity values of the experiment in which the flow is close to maximum are in good correspondence. However, some deviations are visible in the experiment with the highest density values in which the flow is small.

Accordingly, the general course of the fundamental diagram (see figure 15), calculated at the line with the proposed method, is in good correspondence with the classical discrete measurements at the line.

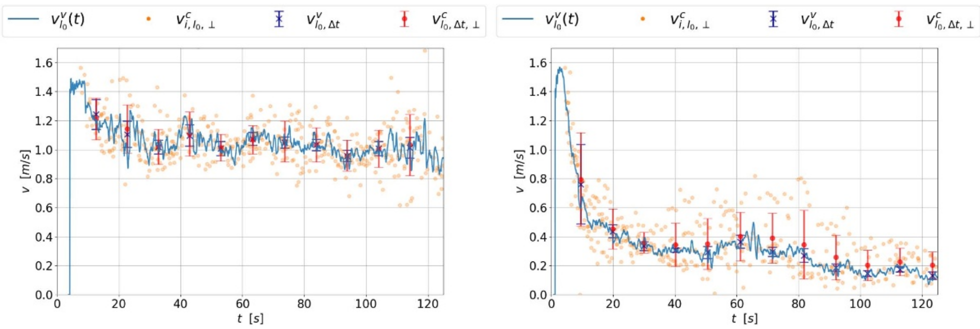

(a) (b)

Figure 14. Speed–time series for the (a) bi_corr_400_03 and (b) bi_corr_400_08 experiments . Comparison between $v^{\mathrm{v}}_{l_0}(t)$ (equation (26)) and the classical individual perpendicular crossing velocity $v^{\mathrm{c}}_{i,l_0,\perp}$. Their mean values within time intervals $\Delta t = 10\,\mathrm{s}$ are $v^{\mathrm{v}}_{l_0,\Delta t}$ and $v^{\mathrm{c}}_{l_0,\Delta t,\perp}$ (equation (5)), respectively.

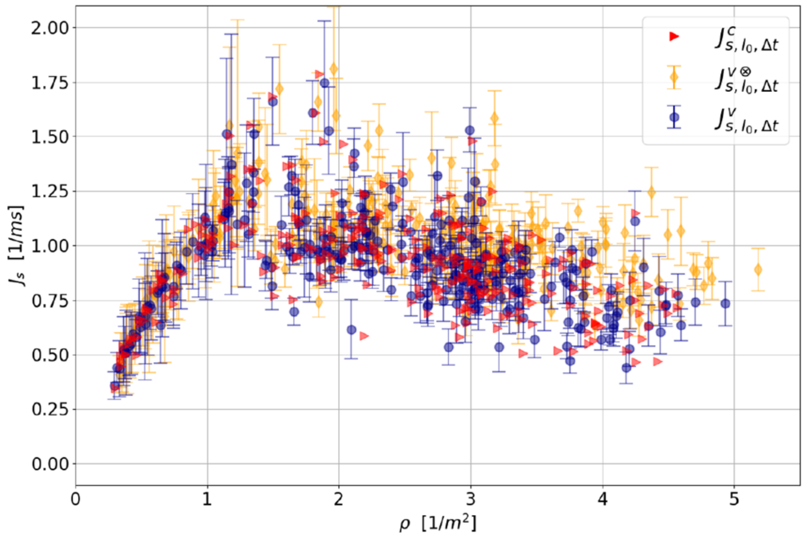

Figure 15. Fundamental diagram for bidirectional flow bi_corr_400 experiments averaged within time intervals of $\Delta t = 5\,\mathrm{s}$. Comparison between the new method in blue (specific flow $J^{\mathrm{v}}_{\mathrm{s},l_0,\Delta t}$ (equation (28)) using line density $\rho^{\mathrm{v}}_{l_0,\Delta t}$ (equation (27))) with classical measurements in red (specific flow $J^{\mathrm{c}}_{\mathrm{s},l_0,\Delta t}$ (equation (3)) and density $\rho^{\mathrm{c}}_{A,\Delta t}$ (equation (7)) within a measurement area with width $\Delta x = 2\,\mathrm{m}$) and a simplified measurement in yellow (with specific flow $J^{\mathrm{v}\otimes}_{\mathrm{s},l_0,\Delta t}$ (equation (48)) and density $\rho^{\mathrm{v}\otimes}_{l_0,\Delta t}$ (equation (45)).

4. Consequences of simplifications of the flow equation

In the previous sections, we discussed how inconsistencies in the definitions of flow, density, and velocity may arise from simplified or non-consistent averaging. The following

J. Stat. Mech. (2026) 043401

analysis quantifies how such simplifications influence the resulting macroscopic quantities. This comparison does not introduce new measurement approaches but demonstrates the practical relevance of the theoretical framework developed above.

In principle, no measurement specification or definition of velocity, density, or flow commonly used in the literature can be called incorrect. Some include more information, others less. Some show large fluctuations, others small. Some emphasise boundary effects, others less, and so on.

In this section, different variants for calculating speed, density, and specific flow at measurement line l_0 are introduced and analysed. These are based on definitions that have been and continue to be used in the literature and may be regarded as simplifications of the definitions introduced in the previous section.

The objective of this section is to quantify the impact of inconsistencies through simplifications, such as the neglect of negative velocities, the utilisation of magnitude as an alternative to orthogonal velocity components, the improper application of velocity and density multiplication, and so forth.

Simplification here means a less unambiguous consideration of information about variables that describe the movement of pedestrians in relation to a measurement line. An example is the magnitude of a velocity vector, which leaves an infinite number of options open with regard to the direction of the movement in relation to the measuring line.

The comparison commences with the most simplistic form of the equation and is refined iteratively to achieve greater alignment with a definition that conforms to the continuity equation.

The comparison starts with speed. First, simply the norm $\|\vec{v}_i(t)\|$ of the individual velocities is considered, and the standard mean value in the form $\bar{x} = \frac{1}{N}\sum_{i=1}^{N} x_i$ is calculated. The resulting speed is denoted as $v_{l_0}^{\mathrm{v}\otimes}(t)$:

$$v_{l_0}^{\mathrm{v}\otimes}(t) = \frac{1}{N_{l_0}(t)} \sum_{\{i|A_i(t)\in l_0\}} \|\vec{v}_i(t)\|. \tag{40}$$

Instead of the standard mean value, the weighting term $\frac{w_i(t)}{w}$ is introduced to represent the integral along the measurement line l_0 and to denote the resulting speed as $v_{l_0}^{\mathrm{v}\dagger}(t)$:

$$v_{l_0}^{\mathrm{v}\dagger}(t) = \sum_{\{i|A_i(t)\in l_0\}} \|\vec{v}_i(t)\| \frac{w_i(t)}{w}. \tag{41}$$

In the next step, only the absolute value of the normal component $|\vec{v}_i(t)\cdot\vec{n}|$ of the velocity is taken into account. The resulting speed is denoted as $v_{l_0}^{\mathrm{v}*}(t)$:

$$v_{l_0}^{\mathrm{v}*}(t) = \sum_{\{i|A_i(t)\in l_0\}} |\vec{v}_i(t)\cdot\vec{n}_{l_0}| \frac{w_i(t)}{w}. \tag{42}$$

As the final step, the norm is omitted to consider the negative contributions of the individual velocities, and the resulting orthogonal speed is denoted as $v^{\mathrm{v}}_{l_0}(t)$:

$$v^{\mathrm{v}}_{l_0}(t) = \sum_{\{i|A_i(t)\in l_0\}} \vec{v}_i(t)\,\vec{n}_{l_0}\frac{w_i(t)}{w}. \tag{43}$$

The definition of $v^{\mathrm{v}}_{l_0}(t)$ is equivalent to the definition in equation (26), which conforms with the continuity equation.

The mean speed $v^{\mathrm{v}}_{l_0,\Delta t}$ within time interval Δt can then be obtained by

$$v^{\mathrm{v}}_{l_0,\Delta t} = \frac{1}{M_{\Delta t}}\sum_{k|t_k\in\Delta t} v^{\mathrm{v}}_{l_0}(t_k) \tag{44}$$

in which $v^{\mathrm{v}}_{l_0}(t_k)$ can be the speed according to equations (40)–(43).

For the calculation of line density $\rho^{\mathrm{v}}_{l_0}(t)$, two strategies may be compared. In the simplified case, the standard mean value of all individual Voronoi densities $\rho^{\mathrm{v}}_i(t)$ is used. The resulting line density is denoted $\rho^{\mathrm{v}\otimes}_{l_0}(t)$:

$$\rho^{\mathrm{v}\otimes}_{l_0}(t) = \frac{1}{N_{l_0}(t)}\sum_{\{i|A_i(t)\in l_0\}} \rho^{\mathrm{v}}_i(t).. \tag{45}$$

Introducing the weighting term $\frac{w_i(t)}{w}$ to represent the line integral results in the density $\rho^{\mathrm{v}}_{l_0}(t)$, which follows the definition of the line density in equation (27):

$$\rho^{\mathrm{v}}_{l_0}(t) = \sum_{\{i|A_i(t)\in l_0\}} \rho^{\mathrm{v}}_i(t)\frac{w_i(t)}{w}. \tag{46}$$

Again, the mean density within time interval Δt is given by

$$\rho^{\mathrm{v}}_{l_0,\Delta t} = \frac{1}{M_{\Delta t}}\sum_{k|t_k\in\Delta t} \rho^{\mathrm{v}}_{l_0}(t_k), \tag{47}$$

where $\rho^{\mathrm{v}}_{l_0}(t_k)$ is the line density at time t_k at l_0 calculated by equation (45) or (46).

Following the strategies to calculate the speed and density, we now consider the same simplifications for the flow.

Only the norm $\|\vec{v}_i(t)\|$ of the individual Voronoi velocities is considered, and the standard mean value for line l_0 is calculated. The resulting specific flow is denoted as $J^{\mathrm{v}\otimes}_{\mathrm{s},l_0}(t)$:

$$J^{\mathrm{v}\otimes}_{\mathrm{s},l_0}(t) = \frac{1}{N_{l_0(t)}}\sum_{\{i|A_i(t)\in l_0\}} \frac{\|\vec{v}_i(t)\|}{A_i(t)}. \tag{48}$$

J. Stat. Mech. (2026) 043401

In the second step, the weighting term $\frac{w_i(t)}{w}$ is used to represent the line integral and to denote the resulting specific flow as $J^{\mathrm{v}\dagger}_{\mathrm{s},l_0}(t)$:

$$J^{\mathrm{v}\dagger}_{\mathrm{s},l_0}(t) = \sum_{\{i|A_i(t)\in l_0\}} \frac{\|\vec{v}_i(t)\|}{A_i(t)} \frac{w_i}{w}. \tag{49}$$

Then, only the norms $\|\vec{v}_i(t)\vec{n}\|$ of the normal components of the individual Voronoi velocities resulting in specific flow $J^{\mathrm{v}*}_{\mathrm{s},l_0}(t)$ are considered as

$$J^{\mathrm{v}*}_{\mathrm{s},l_0}(t) = \sum_{\{i|A_i(t)\in l_0\}} \frac{|\vec{v}_i(t)\cdot\vec{n}|}{A_i(t)} \frac{w_i}{w}. \tag{50}$$

Finally, the individual normal velocities are used as $\vec{v}_i(t)\vec{n}$ to account for negative contributions. The resulting specific flow is denoted as $J^{\mathrm{v}}_{\mathrm{s},l_0}(t)$:

$$J^{\mathrm{v}}_{\mathrm{s},l_0}(t) = \sum_{\{i|A_i(t)\in l_0\}} \frac{\vec{v}_i(t)\,\vec{n}}{A_i(t)} \frac{w_i}{w}, \tag{51}$$

which conforms with the continuity equation definition of the flow in equation (28).

The mean specific flow within time interval Δt is

$$J^{\mathrm{v}}_{\mathrm{s},l_0,\Delta t} = \frac{1}{M_{\Delta t}} \sum_{k|t_k\in\Delta t} J^{v}_{l_0}(t_k), \tag{52}$$

where $J^{\mathrm{v}}_{\mathrm{s},l_0}(t_k)$ is the flow at time t_k at l_0 calculated by equations (48)–(51).

Up to here, the mean value of the product of speed and density $\overline{(\rho\cdot u)}^{\mathrm{v}}_{l_0}$ has been used for the calculation of the local mean value of the specific flow $\overline{J}^{\mathrm{v}}_{\mathrm{s},l_0}$ as in

$$\overline{J}^{\mathrm{v}}_{\mathrm{s},l_0}(t_k) = \overline{(\rho\cdot u)}^{\mathrm{v}}_{l_0}(t_k). \tag{53}$$

If, instead, the product of the individual mean values $\overline{\rho}^{\mathrm{v}}_{l_0}$ and $\overline{u}^{\mathrm{v}}_{l_0}$ is used, as in

$$\overline{J}^{\mathrm{v}}_{\mathrm{s},l_0}(t_k) = \overline{\rho}^{\mathrm{v}}_{l_0}(t_k)\cdot\overline{u}^{\mathrm{v}}_{l_0}(t_k) \tag{54}$$

then the resulting value for $\overline{J}^{\mathrm{v}}_{\mathrm{s},l_0}$ is consistent with that in equation (53) only if there is a linear relationship between velocity and density. This may be the case in the free-flow branch of the fundamental diagram, but even here there are measurements that cast doubt on this. In addition, it is questionable whether a linear dependence can be assumed in the congested branch (higher density). Applying this simplification (equation (54)) on $J^{\mathrm{v}}_{\mathrm{s},l_0}$ and $J^{\mathrm{v}\otimes}_{\mathrm{s},l_0}$ yields

$$J^{\mathrm{v}'}_{\mathrm{s},l_0}(t) = \left[\sum_{\{i|A_i(t)\in l_0\}} \vec{v}_i(t)\,\vec{n}\frac{w_i}{w}\right]\cdot\left[\sum_{\{i|A_i(t)\in l_0\}} \frac{1}{A_i(t)}\frac{w_i}{w}\right] \tag{55}$$

Table 1. RMS deviation (equation (57)) between the time averages (equation (52)) calculated for the different simplifications of the specific flow and the classical specific flow $J^{\mathrm{c}}_{\mathrm{s},l0,\Delta t}$ (equation (3)) measured at the same time intervals for different experimental datasets. With an increasing degree of simplification, the RMS value increases.

Experiment	$J^{\mathrm{v}\otimes\prime}_{\mathrm{s},l_0}$ (%)	$J^{\mathrm{v}\otimes}_{\mathrm{s},l_0}$ (%)	$J^{\mathrm{v}\dagger}_{\mathrm{s},l_0}$ (%)	$J^{\mathrm{v}*}_{\mathrm{s},l_0}$ (%)	$J^{\mathrm{v}}_{\mathrm{s},l_0}$ (%)
uni_corr_03	6.5	6.0	1.9	1.9	1.9
uni_corr_10	143.1	122.2	117.7	45.0	12.3
bi_corr_03	7.6	6.6	1.3	1.1	1.1
bi_corr_08	33.3	23.3	23.4	4.0	3.4

and

$$J^{\mathrm{v}\otimes\prime}_{\mathrm{s},l_0}(t) = \left[\frac{1}{N_{l_0(t)}} \sum_{\{i|A_i(t)\in l_0\}} \|\vec{v}_i(t)\|\right] \cdot \left[\frac{1}{N_{l_0(t)}} \sum_{\{i|A_i(t)\in l_0\}} \frac{1}{A_i(t)}\right]. \tag{56}$$

Using the experimental data as an example, we now examine the extent to which the individual simplifications change the values for density, velocity, and flow. An overview is given in table 1, summarising the agreement between the flow calculations and the classical flow measurements on the line. This was done by calculating the root mean square (RMS) between the time averages of the calculated data (equation (52)) and the classical flow $J^{\mathrm{c}}_{\mathrm{s},l_0,\Delta t}$ (equation (3)) measured at the same time intervals. The RMS was calculated as follows:

$$\mathrm{RMS} = \sqrt{\frac{1}{N}\sum_{n=1}^{N} \frac{\left[J^{\mathrm{v}}_{\mathrm{s},l_0,\Delta t}(\Delta t_n) - J^{\mathrm{c}}_{\mathrm{s},l_0,\Delta t}(\Delta t_n)\right]^2}{\left[J^{\mathrm{c}}_{\mathrm{s},l_0,\Delta t}(\Delta t_n)\right]^2}} \tag{57}$$

where N is the number of time intervals Δt during the experiment. In principle, table 1 shows that every simplification leads to an increase in the RMS value and thus to a discrepancy with the classic flow measurement $J^{\mathrm{c}}_{\mathrm{s},l_0,\Delta t}$. The definition $J^{\mathrm{v}}_{\mathrm{s},l_0}$ has the lowest RMS value for all experiments. The high RMS values for the uni_corr_10 experiment can be explained by the very low flow near zero (standstill). It should be reconsidered how to deal with multiple crossings of the measurement line by one person in classic flow measurements (see last sentence in the paragraph below equation (3)).

The following comparison of measurement methods is used to analyse the consistency between direct and indirect measurements of the variables, such as $J = \frac{\Delta N}{\Delta t}$ to $J = f(\rho, v)$ in the form of time series. The differences in the calculation simplifications are less clear in the experiments with low density and high flux (uni_corr_500_03 and bi_corr_400_03). With high density and small flow (uni_corr_500_10and bi_corr_400_08), however, they are sometimes significant. We therefore focus on these experiments, as shown in figure 16.

In the case of density, the differences caused by using the weighting term are notable. The effect of the weighting is a smoother curve, and the density is lower (see $\rho^{\mathrm{v}\otimes}_{l_0}$).

J. Stat. Mech. (2026) 043401

Figure 16. Comparison of time series of density, speed, and specific flow applying the different simplifications on corridor experiments. Left column: unidirectional experiment uni_corr_500_10; right column: bidirectional experiment bi_corr_400_08.

The order of averaging and multiplication in calculating the specific flow (difference between $J^{\mathrm{v}\otimes\prime}_{\mathrm{s},l_0}$ and $J^{\mathrm{v}\otimes}_{\mathrm{s},l_0}$) has the greatest influence at high densities. This can be seen in the example of bi_corr_400_08, in which the mean value $J^{\mathrm{v}\otimes\prime}_{\mathrm{s},l_0}$ (following equation (54)) generally results in higher flow values than the mean value $J^{\mathrm{v}\otimes}_{\mathrm{s},l_0}$ (following equation (53)). Otherwise, the effect is less pronounced.

The remaining observations on speed and flow can be summarised together, as the effects of the simplifications on them are similar. The difference between $\mathrm{v}^{\otimes}$ and $\mathrm{v}^{\dagger}$ is the weighting of the contributions of the pedestrian i ($1/N$ or w_i/w). The effect is mainly a smoothing (as with density). Using the normal component of speed (transition from $\mathrm{v}^{\dagger}$ to v^{*}) has the greatest effect. The effect is most evident for the bi_corr_400_08 experiment in the range $t = 50 - 55$ s. If $\|\vec{v}\|$ is used ($v^{\mathrm{v}\dagger}_{l_0}$ and $J^{\mathrm{v}\dagger}_{\mathrm{s},l_0}$), the specific flow increases to approximately $1.4\,\mathrm{m\,s^{-1}}$, whereas it drops to almost $0.4\,\mathrm{m\,s^{-1}}$ if the normal

J. Stat. Mech. (2026) 043401

velocity component is used ($v_{l_0}^{\mathrm{v}^*}$ and $J_{\mathrm{s},l_0}^{\mathrm{v}^*}$). The significance of this effect is also reflected in table 1. Finally, versions v^* and v differ only in the use of the magnitude $|\vec{v}\cdot\vec{n}|$ or the sign of the vertical velocity $\vec{v}\cdot\vec{n}$. In most cases, the two calculated velocities ($v_{l_0}^{\mathrm{v}^*}$ and $v_{l_0}^{\mathrm{v}}$) and specific flows ($J_{\mathrm{s},l_0}^{\mathrm{v}^*}$ and $J_{\mathrm{s},l_0}^{\mathrm{v}}$) agree very well. However, there are two cases that we would like to draw attention to:

1. In the uni_corr_500_10 experiment in the range $t = 80 - 85$ s, a negative velocity $v_{l_0}^{v}$ and therefore a negative specific flow $J_{\mathrm{s},l_0}^{\mathrm{v}}$ are measured. This is exactly one of the cases we wanted to make detectable with the proposed measurement method.
2. In the bi_corr_400_08 experiment at approximately $t = 65 - 70$ s, an increase in velocity is measured for $v_{l_0}^{\mathrm{v}^*}$, whereas $v_{l_0}^{\mathrm{v}}$ drops significantly. After comparing the graphs in figure 16 and the RMS errors in table 1, it can be summarised that the calculated values decrease from $\mathrm{v}^{\otimes\prime}$ to v, and the agreement with the flow measured on the line improves from $\mathrm{v}^{\otimes\prime}$ to v. The largest step occurs from $\mathrm{v}^{\dagger}$ to v^* (as described above).

For more information regarding the full range of the fundamental diagram, refer to figures 11 and 15, where the fundamental diagrams measured with simplified methods are included.

5. Summary and conclusions

The measurement methods and the method of calculating variables in pedestrian dynamics have not kept pace with the development and precision of data trajectory recordings. The classical flow equation has been used repeatedly, even though it presents issues as discussed in section 2.2. First, the flow equation does not specify how the scalar velocity is calculated from the given velocity vector. Therefore, it is unclear if and how negative contributions to the flow are taken into account. Second, density is usually measured as an average over a two-dimensional area. Inhomogeneities are not taken into account, and spatial averages (density) are combined with temporal averages (flow). Third, multiplication by the length of the measurement line implies that the product of density and velocity along the measurement line is constant. Fourth, when using the flow equation to calculate the flow from measured values of density and velocity, one must be aware that the multiplication of the mean values of density and velocity does not necessarily equal the mean value of density times velocity.

The problems listed above show that previous measurements of flow, density, and speed measured by trajectories of the head do not necessarily conform to the continuity equation. The continuity equation is a conservation law describing changes in density and velocity in time and space, ensuring that no pedestrian is born or turns to dust (conserving the number of pedestrians). These problems lead to inaccuracies or uncertainties in the fundamental diagrams, which can lead to misinterpretation of important crowd conditions. For example, it can lead to misjudgements about how and when crowds can come to a standstill. This, in turn, can lead to an incorrect estimation of maximum density or misjudgement of critical situations. In practice, however, precise people counting is still a helpful tool for determining the current throughput per hour.

In this paper, a framework was introduced that defines density, speed, and flow on the basis of trajectories in accordance with the continuity equation. To relate the field representation of the continuity equation to the discrete trajectories of pedestrians, a Voronoi decomposition was applied. A method was proposed to measure density, speed, and flow on a line and to deal with different main directions of motion (without losing the sign of the velocity vector). The newly introduced measurement method was applied to precise empirical data from laboratory experiments. The results were compared with classical measurements, and the effects of various simplifications of the measurement method on the results were analysed. This shows that there are density ranges in which the influence of the measurement method is small (especially in the free-flow branch). In the high-density range, however, the difference is clearly recognisable. This is the density range in which, for example, stop-and-go waves and thus a heterogeneous distribution of density, velocity, and flow can occur.

It should be noted that the method introduced measures the flow perpendicular to a measuring line. In cases in which the performance in multidimensional traffic must be determined, careful consideration is required in placing the measuring line in a meaningful way. The number, length, and positioning of measuring lines are completely free and guaranteed to conform to the continuity equation. This method makes it possible to define measuring lines of any length and complexity at all possible positions within the system.

To further investigate the benefits of the newly proposed measurement method, new empirical studies are necessary. These experiments should involve transitions between a moving mode and a stopping mode (and vice versa). The result should be a more accurate dataset of the high-density area of the fundamental diagram. This should be applied to unidirectional, bidirectional, and multidirectional pedestrian flows. These data and measurement methods will provide new and precise information on high-density conditions, such as stop-and-go waves or pushing crowds in which transversal density waves are observable. These findings have the potential to enhance crowd safety.

Acknowledgments

The authors would like to thank Tobias Schrödter and Christian Hirt for implementing the new measurement method in the software PedPy [40].

Funding acknowledgments

This research was funded by the Deutsche Forschungsgemeinschaft (DFG, German Research Foundation) under Project DenseDynamics (549018809).

References

[1] Predtechenskii V M and Milinskii A I 1978 *Planing for Foot Traffic Flow in Buildings* (Amerind Publishing) (Translation of: Proekttirovanie Zhdanii s Uchetom Organizatsii Dvizheniya Lyuddskikh Potokov, Stroiizdat Publishers, Moscow, 1969)

[2] Fruin J J 1971 *Pedestrian Planning and Design* (Elevator World)

[3] Buchmueller S and Weidmann U 2006 Parameters of pedestrians, pedestrian traffic and walking facilities *IVT Schriftenreihe* **132**

[4] Nelson H E and Mowrer F W 2002 Emergency movement *Sfpe Handbook of Fire Protection Engineering* ed P J DiNenno (National Fire Protection Association) ch 14, pp 367–80

[5] Schreckenberg M and Sharma S D (eds) 2002 *Pedestrian and Evacuation Dynamics* vol 1 (Springer)

[6] Song W, Ma J and Fu L 2017 Proceedings of pedestrian and evacuation dynamics 2016 *Collect. Dyn.* **1** 618

[7] Edie L C 1963 Discussion of traffic stream measurements and definitions *Proc. 2nd Int. Symp. Theory of Traffic Flow* ed J Almond pp 139–54

[8] Henderson L R F 1974 On the fluid mechanics of human crowd motion *Transp. Res.* **8** 509–15

[9] Hughes R L 2002 A continuum theory for the flow of pedestrians *Transp. Res. B* **36** 507–35

[10] Bellomo N and Dogbe C 2011 On the modeling of traffic and crowds: a survey of models, speculations and perspectives *SIAM Rev.* **53** 409–63

[11] Hankin B D and Wright R A 1958 Passenger flow in subways *Oper. Res. Q.* **9** 81–88

[12] Hoell L A 1968 Pedestrian travel rates in central business districts *Traffic Eng.* **38** 10–13

[13] Navin F D and Wheeler R J 1969 Pedestrian flow characteristics *Traffic Eng.* **39** 30–36

[14] Tanaboriboon Y, Hwa S S and Chor C H 1986 Pedestrian characteristics study in Singapore *J. Transp. Eng.* **112** 229–35

[15] Helbing D, Johansson A and Al-Abideen H Z 2007 Dynamics of crowd disasters: An empirical study *Phys. Rev. E* **75** 046109

[16] Steffen B and Seyfried A 2010 Methods for measuring pedestrian density, flow, speed and direction with minimal scatter *Physica A* **389** 1902–10

[17] Zhang J, Klingsch W, Schadschneider A and Seyfried A 2011 Experimental study of pedestrian flow through a T-junction *Traffic and Granular Flow 2011* (arXiv:1207.5688)

[18] Cao S, Seyfried A, Zhang J, Holl S and Song W 2017 Fundamental diagrams for multidirectional pedestrian flows *J. Stat. Mech.* 033404

[19] Cao S, Lian L, Chen M, Yao M, Song W and Fang Z 2018 Investigation of difference of fundamental diagrams in pedestrian flow *Physica A* **506** 661–70

[20] Boltes M, Zhang J, Tordeux A, Schadschneider A and Seyfried A 2018 Empirical results of pedestrian and evacuation dynamics *Encyclopedia of Complexity and Systems Science* ed R A Meyers (Springer) pp 1–29

[21] Haghani M 2020 Empirical methods in pedestrian, crowd and evacuation dynamics: part I. Experimental methods and emerging topics *Saf. Sci.* **129** 104743

[22] Feng Y, Duives D, Daamen W and Hoogendoorn S 2021 Data collection methods for studying pedestrian behaviour: a systematic review *Build. Environ.* **187** 107329

[23] Seyfried A, Boltes M, Kähler J, Klingsch W, Portz A, Rupprecht T, Schadschneider A, Steffen B and Winkens A 2010 Enhanced empirical data for the fundamental diagram and the flow through bottlenecks *Pedestrian and Evacuation Dynamics 2008* ed W W F Klingsch, C Rogsch, A Schadschneider and M Schreckenberg (Springer) pp 145–56

[24] Zhang J, Cao S, Salden D and Ma J 2016 Homogeneity and activeness of crowd on aged pedestrian dynamics *Proc. Comput. Sci.* **83** 361–8

[25] Ren X, Zhang J and Song W 2019 Contrastive study on the single-file pedestrian movement of the elderly and other age groups *J. Stat. Mech.* 093402

[26] Subaih R, Maree M, Chraibi M, Awad S and Zanoon T 2020 Experimental investigation on the alleged gender-differences in pedestrian dynamics: a study reveals no gender differences in pedestrian movement behavior *IEEE Access* **8** 33748–57

[27] Ziemer V 2019 Mikroskopische Fundamentaldiagramme der Fußgängerdynamik—Empirische Untersuchung von Experimenten eindimensionaler Bewegung sowie quantitative Beschreibung von Stau-Charakteristika *PhD Thesis* Bergische Universität Wuppertal

[28] Jelić A, Appert-Rolland C, Lemercier S and Pettré J 2012 Properties of pedestrians walking in line: fundamental diagrams *Phys. Rev. E* **85** 036111

[29] Cao S, Zhang J, Salden D, Ma J, Shi C'an and Zhang R 2016 Pedestrian dynamics in single-file movement of crowd with different age compositions *Phys. Rev. E* **94** 012312

J. Stat. Mech. (2026) 043401

[30] Subaih R, Maree M, Chraibi M, Awad S and Zanoon T 2019 Gender-based insights into the fundamental diagram of pedestrian dynamics *Computational Collective Intelligence* ed N T Nguyen, R Chbeir, E Exposito, B Aniorté and P vand Trawiński (Springer) pp 613–24
[31] Cao S, Zhang J, Song W, Shi C'an and Zhang R 2018 The stepping behavior analysis of pedestrians from different age groups via a single-file experiment *J. Stat. Mech.* 033402
[32] Cao S, Wang P, Yao M and Song W 2019 Dynamic analysis of pedestrian movement in single-file experiment under limited visibility *Commun. Nonlinear Sci. Numer. Simul.* **69** 329–42
[33] Zhang J, Tordeux A and Seyfried A 2014 Effects of boundary conditions on single-file pedestrian flow *Cellular Automata* (Springer) pp 462–9
[34] Zhang J, Mehner W, Holl S, Boltes M, Andresen E, Schadschneider A and Seyfried A 2014 universal flow-density relation of single-file bicycle, pedestrian and car motion *Phys. Lett. A* **378** 3274–7
[35] Zhang J, Klingsch W, Schadschneider A and Seyfried A 2012 Ordering in bidirectional pedestrian flows and its influence on the fundamental diagram *J. Stat. Mech.* P02002
[36] Holl S 2016 Methoden für die Bemessung der Leistungsfähigkeit multidirektional genutzter Fußverkehrsanlagen *PhD Thesis* Bergische Universität Wuppertal
[37] Zhang J, Wang Q, Hu Y, Cao S, Xia L and Song W 2018 The effect of a directional split flow ratio on bidirectional pedestrian streams at signalized crosswalks *J. Stat. Mech.* 073408
[38] Feliciani C and Nishinari K 2016 Empirical analysis of the lane formation process in bidirectional pedestrian flow *Phys. Rev. E* **94** 032304
[39] Johansson A, Helbing D, Al-Abideen H Z and Al-Bosta S 2008 From crowd dynamics to crowd safety: a video-based analysis *Adv. Complex Syst.* **11** 497–527
[40] Schrödter T (The PedPy Development Team) 2024 PedPy—pedestrian trajectory analyzer (https://doi.org/10.5281/zenodo.11778532)

J. Stat. Mech. (2026) 043401